

# Raman spectroscopy of primary bovine aortic endothelial cells: a comparison of single cell and cell cluster analysis

A. R. Boyd · L. L. McManus · G. A. Burke ·  
B. J. Meenan

Received: 7 March 2011 / Accepted: 4 June 2011 / Published online: 14 June 2011  
© Springer Science+Business Media, LLC 2011

**Abstract** There are many techniques that allow in vitro interactions among cells and their environment to be monitored, including molecular, biochemical and immunochemical techniques. Traditional techniques for the analysis of cells often require fixation or lysis from substrates; however, use of such destructive methods is not feasible where the expanded cell cultures are required to be used for clinical implantation. Several studies have previously highlighted the potential of Raman spectroscopy to provide useful information on key biochemical markers within cells. As such, we highlight the capability of Raman spectroscopy with different laser spot sizes for use as a non-invasive, rapid, and specific method to perform in situ analysis of primary bovine aortic endothelial cells (BAECs). Raman spectra were collected from both individual live cells cultured on fused silica substrates and on clusters of live cells placed on fused silica substrates, measured at 532 and 785 nm. The results obtained show notable spectral differences in DNA/RNA region indicative of the relative cytoplasm and nucleus contributions. Raman spectra of cell clusters show slight variations in the intensity of the phenylalanine peak ( $1004\text{ cm}^{-1}$ ) indicating variations in protein contribution. These spectra also highlight contributions from other cellular components such as, proteins, lipids, nucleic acids and carbohydrates, respectively.

## 1 Introduction

Tissue loss and organ failure accounts for nearly half of medical expenditure, thereby making it one of the most

costly problems in healthcare today. In the US alone, \$400 billion dollars is spent annually on those suffering from organ failure or tissue loss. As such, there is an ever increasing patient need for biological substitutes to replace or repair organ/tissue function due to damage caused by disease or trauma [1].

In order to achieve a successful clinical outcome it is envisaged that any regenerative medicine product needs a source of healthy and expandable cells that are qualified for clinical application. In the case of tissue engineered products, suitable scaffolds and automated cell culture systems/bioreactors optimised for the task are also required. Within this environment cells are seen as the functional elements of repair and regeneration and the scaffold as the initial 3D mechanical construct. As a result it is important that the appropriate cells can be sourced, cultivated and expanded in vitro to attain the appropriate phenotype or function and that this process can be completed accurately and repeatedly prior to transplantation. However, during the expansion and cell culture process, complex cell biological processes and sub-cellular components must be monitored [2–4].

A core tenant for the expansion of a cell population for regenerative medicine is the ability to provide a fit-for-purpose system to monitor cell status (cell viability, phenotype, etc.), from the point of view of sourcing the cells right through to applying them in a clinical setting. In this regard, the method of assessment should be non-invasive, rapid, specific and should also have the ability to perform in situ analysis of the function of growing tissues at a cellular level [5–7]. Biochemical and genomic changes are at present monitored using chemical assays, Immunocytochemistry, confocal microscopy and modular biological analysis such as flow cytometry, conventional real-time polymerase chain reaction (PCR) and cDNA microarray analysis. These methods do provide comprehensive

---

A. R. Boyd (✉) · L. L. McManus · G. A. Burke · B. J. Meenan  
Nanotechnology and Integrated Bioengineering Centre (NIBEC),  
University of Ulster, Shore Road, Newtownabbey, Antrim BT37  
0QB, Northern Ireland  
e-mail: ar.boyd@ulster.ac.uk

information; however, they are also time consuming, performed over several days and require labels or biomarkers that render the cells unsuitable for further use. Consequently a rapid, non-invasive, label-free diagnostic tool would be of major benefit here [7–9].

There are several optical and biological techniques, including, bioluminescence imaging (BI), optical coherence tomography (OCT), surface plasmon resonance (SPR), fourier transform spectroscopy (FTIR), which can be utilised in order to examine cellular behaviours whilst in culture [5, 10]. However, due to the complexity of cells the requirements needed to monitor cells in culture are extending rapidly and some of the optical techniques are not up to standard therefore alternatives are needed. Raman spectroscopy is a vibrational spectroscopic technique offers many benefits over the traditional methods due to its non-destructive and non-invasive analysis at a cellular level. However, the analysis method itself could induce biochemical changes in cellular characteristics. To avoid this, the optical platform must be optimised and the conditions, such as, laser wavelength, laser power and exposure times monitored and controlled [11]. Extensive research by Puppels et al. has demonstrated the efficacy of using Raman spectroscopy to study living cells and chromosomes for the characterisation of the cytoplasm and nucleus in human white blood cells [6, 12]. Similarly, literature published by Notingher et al. [13] reported the use of Raman spectroscopy for analyses of various positions within a single cell. More recently, Raman spectroscopy has been utilised to detect changes in cells during the cell cycle [9, 14, 15], cell death [6–8, 13, 16, 17], cell differentiation [18–20], cell proliferation [14], bone cell mineralisation [13, 21] and mitosis [22, 23].

The purpose of this study was to examine live single cells and cell clusters of primary bovine aortic endothelial cells (BAECs) in a non-destructive manner using different Raman platforms capable of delivering data that can discriminate cellular composition and sub-cellular components. BAECs are isolated from the bovine aorta and are useful for studying vascular diseases such as thrombosis, atherosclerosis and hypertension. Typically primary cells are the ideal model for *in vitro* studies, however, it should be noted that their use can be limited elsewhere due to a slow growth rate, loss of phenotype and limited life span in culture.

## 2 Materials and methods

### 2.1 Primary bovine aortic endothelial cells

The endothelium is the thin layer of endothelial cells that line the interior surface of the blood and lymphatic

system—from the aorta to the smallest capillaries. Primary BAECs isolated directly from a fresh bovine aorta were used in this study. Briefly, endothelial cells were obtained from bovine aorta by mild treatment with collagenase and medium perfusion, according to previously described methods with minor modifications [24, 25]. Cells were grown in a humidified incubator at 37°C with 5% CO<sub>2</sub> in minimum essential media (MEM, Sigma, UK) that was supplemented with 10% Foetal Calf Serum (FCS) and 1% gentamycin sulphate in a humidified incubator (all obtained from invitrogen, UK). The cells were maintained cultured to sub-confluency and passaged every 3–4 days using 0.25% trypsin–EDTA (Sigma, UK). The cells were seeded on fused silica substrates at a seeding density of approximately 100,000/cm<sup>2</sup>.

### 2.2 Immunofluorescence staining

Cells were seeded onto 15 mm × 15 mm × 1.2 mm fused silica substrates (The Technical Glass Company, UK), and cultured under normal conditions at 37°C for 48 h. Immunofluorescence staining was performed to examine the morphology of the cells. After 48 h, the cells were rinsed in ice-cold PBS, fixed and permeabilised in 3.7% paraformaldehyde (PFA) containing 0.1% Triton X-100 for 20 min at 4°C, then washed 3 times for 15 min in PBS in order to remove traces of PFA. To visualise actin, the cell actin cytoskeleton was stained with Alexa Fluor 488 phalloidin probe and the cell nuclei with DAPI nucleic acid stain (Molecular Probes, Inc., Invitrogen). After washing twice for 5 min in PBS, the substrates were mounted in glycerol media (Vector Laboratories, UK). The substrates were sealed using a clear varnish and they were examined using a Carl Zeiss LSM5 Pascal (Carl Zeiss MicroImaging, Germany) confocal scanning laser microscope (CLSM).

### 2.3 Raman spectroscopy of single cells

For analysis of single BAECs, cells were grown to confluency as outlined previously and seeded onto fused silica substrates for 48 h. Samples were washed and gently rinsed in PBS to remove any unattached cells. Various positions within a single cell were analysed, including the cell nucleus and cytoplasm.

Raman spectroscopy was performed on individual cells using a confocal XploRA Raman microscope (Horiba Jobin–Yvon). The system was equipped with a 532 nm laser module with high stability Edge and Interface filters set at 532 nm for measurements from 150 cm<sup>-1</sup>. Single cells were analysed using the integrated confocal Raman microscope with a 100× objective lens to focus on the cell to ensure optimal positioning and signal-to-noise ratio. The nominal spot size at the sample was assessed to be ~ 1 μm,

and the power of the laser beam focused on the sample was 20 mW. Spectra were collected from both the nuclei ( $n = 4$ ) and cytoplasm ( $n = 4$ ) from within individual cells ( $n = 15$ ). Scans were recorded from a spectral range of  $3600\text{--}200\text{ cm}^{-1}$ , and Raman backscattered light from each point of the cell was averaged over  $2 \times 10\text{ s}$  and collected through the same objective.

#### 2.4 Raman spectroscopy of cell clusters

In order to analyse the cells using a Raman spectrometer, the BAECs were grown to confluence as outlined previously. Cells were trypsinised, centrifuged at low speed and re-suspended in media for 1 h. After this, the suspension was centrifuged at 5,000 rpm in order to produce a cell cluster suitable for analysis using the Raman spectrometer. Cell clusters were placed on fused silica and analysed immediately.

Raman spectroscopy was performed on the cell clusters using a Raman station, (PerkinElmer Ltd, UK) equipped with a stabilised 785 nm near-infrared (NIR) diode laser. Laser power was 100 mW at the cell cluster. Cell clusters were analysed in triplicate using an autofocus routine for each sample to ensure optimal sample positioning and signal-to-noise ratio. In order to account for sample inhomogeneity the instrument was configured for macro-sampling therefore, allowing the collection of Raman scattering from 100  $\mu\text{m}$  diameter spot. Scans were recorded from 3600 to  $200\text{ cm}^{-1}$  with up to a  $3 \times 40\text{ s}$  exposures utilising a laser power of 100 mW. The instrument was wavelength calibrated using a neon source and verified using a polystyrene secondary standard [American society for testing and materials (ASTM) E 1840-96].

#### 2.5 Data pre-processing

It is accepted that spectral artefacts can have a considerable effect on the interpretation of data. Therefore, it is necessary to distinguish between biochemical information and undesired effects. With Raman spectroscopy, it is known that before data interpretation can be performed, pre-processing of data should be carried out. To this end Origin 7 software (OriginLab, USA) was used to routinely pre-process the raw data. In the first instance, band alignment was performed to correct for instrumental spectral shifts. As such all spectra were normalised using the area of the  $1449\text{ cm}^{-1}$  band. A multipoint baseline correction and smoothing by a 5-point Savitzky-Golay filter was also employed for each Raman spectra. Contributions of the fused silica substrate were subtracted, however, small contributions may still be present. The area of individual vibrational bands was computed using the curve-fitting option of Origin 7 software.

### 3 Results and discussion

#### 3.1 Cell morphology and immunofluorescence

To ensure BAECs exhibited typical morphological characteristics during culture their morphology was determined using a phase contrast microscope. When confluent BAECs exhibited expected morphology for endothelial cells and were generally cuboidal-like in shape showing little or no cellular overlap, with frequently vacuolated junctions. When in culture a small number of cells lost their initial ‘cobblestone’ appearance and became flat and elongated, however, this was not entirely unexpected. In addition to the monitoring of the cell morphology during culture using phase contrast microscopy, immunofluorescence staining of the cells was also undertaken using 488 phalloidin and DAPI after culture in normal media for 48 h. In the case of the BAECs investigated here they typically exhibited the expected cuboidal-like cell morphology at confluency as shown in Fig. 1.

#### 3.2 Raman spectroscopy of primary bovine aortic endothelial cells

##### 3.2.1 Single cell analysis

Raman spectroscopy was used to distinguish between different positions within the same cell, namely the cytoplasm and the nucleus. An image showing the morphology of the BAEC growing on the fused silica substrates is shown in Fig. 2. Position  $X_1$  is representative of a typical analysis spot from the cell cytoplasm and position  $X_2$  representative of a typical analysis spot from the cell nucleus. The averaged spectral signatures of the nucleus and cytoplasm for

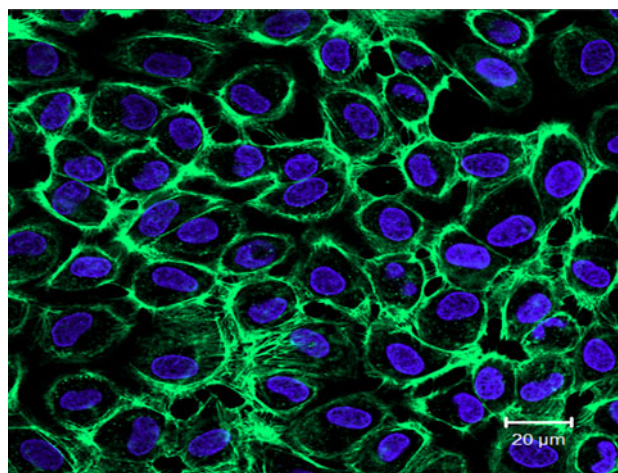


**Fig. 1** Immunofluorescence staining of 488 phalloidin and DAPI in BAECs cultured on fused silica substrates in normal media for 48 h (scale bar 20  $\mu\text{m}$ )

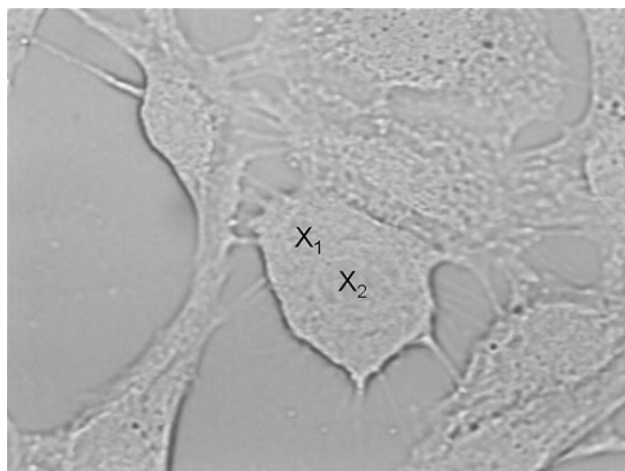


**Fig. 2** A single bovine aortic endothelial cell, X<sub>1</sub> and X<sub>2</sub> marks both the cytoplasm and nucleus respectively (magnification 100 $\times$ )

an individual bovine aortic endothelial cell are illustrated in Fig. 3a, b, respectively. In general, the spectra from both the cytoplasm and nucleus indicate significant contributions from proteins, lipids, DNA/RNA and carbohydrate components and are comparable to those observed previously by others [6–9, 13, 26]. These include typical protein peaks, such as those observed at 937  $\text{cm}^{-1}$  for the C–C backbone, 1004  $\text{cm}^{-1}$  for Phenylalanine, 1200–1300  $\text{cm}^{-1}$  for Amide III, 1320 and 1340  $\text{cm}^{-1}$  for C–H deformations and 1665  $\text{cm}^{-1}$  for Amide I [6–8, 13, 26]. Lipid peaks are also observed at 730  $\text{cm}^{-1}$  for C–N head groups, between 1067 and 1081  $\text{cm}^{-1}$  for the chain C–C stretch and 1132  $\text{cm}^{-1}$  for the C–C stretch (which may also be a consequence of a C–N protein vibration). Peaks indicative of carbohydrates can also be seen at  $\sim 1060$ – $1095 \text{ cm}^{-1}$  for the C–O and C–C stretches, 1420–1480  $\text{cm}^{-1}$  and 1340  $\text{cm}^{-1}$  for the C–H deformations along with significant C–H stretching bands between 2800 and 3050  $\text{cm}^{-1}$  (not shown in spectra here) [26]. It is important to note that there are significant overlaps between the peaks indicative of proteins, carbohydrates, lipids and DNA/RNA as highlighted by Table 1.

The spectra corresponding to cell nuclei contains peaks which are indicative of DNA and RNA at 788, 826 and 855  $\text{cm}^{-1}$  for the O–P–O stretching of the DNA, 1095  $\text{cm}^{-1}$  for the DNA phosphodioxy group  $\text{PO}_2^-$  stretching, 1212–1390 and 1575  $\text{cm}^{-1}$  for adenine, guanine and thymine, as shown in Fig. 3a [27]. However, in the spectra obtained from the cytoplasm, the corresponding DNA/RNA peaks are much weaker than those observed from the nuclei, as shown in Fig. 3b. It is therefore evident that the nucleus contains a significantly increased amount of RNA and DNA as would be expected [13].

Peak fitting routines were performed on the 770–810 and 1020–1160  $\text{cm}^{-1}$  spectral regions, which normally contain

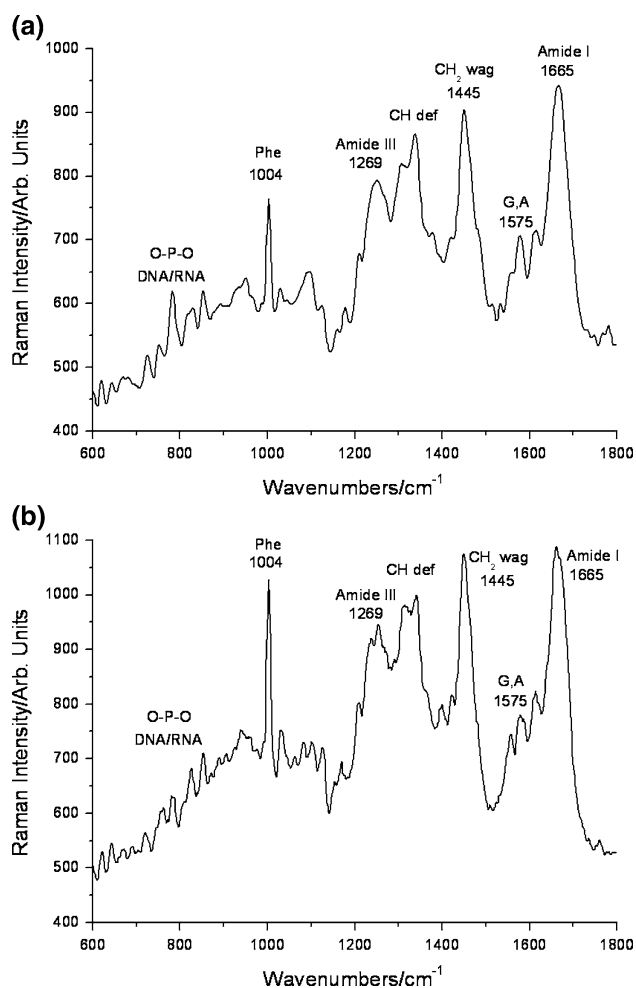


**Fig. 3** Raman spectrum of the **a** nucleus and **b** cytoplasm for an individual bovine aortic endothelial cell

peaks predominantly associated with DNA and RNA. Figure 4 shows peak fitting of the 770–810  $\text{cm}^{-1}$  region corresponding to the (a) nucleus, (b) cytoplasm and the 1020–1160  $\text{cm}^{-1}$  region corresponding to the (c) nucleus, (d) cytoplasm. The peak fitting for the cytoplasm spectra (Fig. 4b) has been fitted with two peaks assigned to ring breathing of cytosine and thymine at 782  $\text{cm}^{-1}$  and the O–P–O stretching of DNA phosphodiester bonds at 788  $\text{cm}^{-1}$  [8, 27]. For the nucleus (Fig. 4a), five peaks have been identified corresponding to O–P–O stretching of DNA phosphodiester bonds at 788  $\text{cm}^{-1}$ , the ring breathing of cytosine and thymine at 782  $\text{cm}^{-1}$ , and peaks at 791, 795 and 803  $\text{cm}^{-1}$ , which are associated with O–P–O stretching of phosphodiester bonds [8, 27]. The 1020–1160  $\text{cm}^{-1}$  region for both the nucleus and the cytoplasm (Fig. 4c, d, respectively) have both been fitted with a series of peaks, including the vibrations of C–O in deoxyribose at 1049  $\text{cm}^{-1}$ ; C–N in proteins at 1128  $\text{cm}^{-1}$ ; vibrations of C–C from lipids at 1066 and 1079  $\text{cm}^{-1}$  and the vibrations of the phosphodioxy groups ( $\text{PO}_2^-$ ) of the DNA backbone at

**Table 1** Peak assignments for primary bovine aortic endothelial cells

Assignment				
Peak position (cm <sup>-1</sup> )	Proteins	DNA/RNA	Lipids	Reference
1749			>C=O ester	[32, 33]
1657	Amide I			[17, 33–35]
1616	C=C Tyr, Trp			[33]
1604	Phe, Tyr			[33]
1576		G, A		[17]
1463	C–H def			[33]
1448	C–H def			[33]
1378		T, A, G		[36]
1368			Sym. Str. CH <sub>3</sub>	[32]
1345	C–H def	A		[17, 36]
1319	C–H def	G		[17, 36]
1304	CH <sub>2</sub> def	A	CH <sub>2</sub> Twist	[17, 33, 35, 37, 38]
1258	Amide III	A		[17]
1240	Amide III	A		[17]
1227	C–H in-plane Phe			[35, 37]
1207	Phe, Tyr			[17, 37]
1178	C–H in-plane bend Tyr			[37]
1152	C–C/C–N str	Ribose-phosphate		[17, 37]
1132	C–C/C–N str		C–C str	[33, 35]
1096		Phosphodioxy group PO <sub>2</sub> <sup>-</sup>	Chain C–C str	[32]
1067	C–N str		Chain C–C str	[33, 35]
1036	C–H in-plane Phe			[35, 37]
1004	Sym. Ring br phe			[17]
985			C–C head groups	[36, 39]
939	Skel. C–C Str			[34]
898		Backbone deoxyrib		[17]
857	Tyr			[17]
835		Ribose-phosphate		[17]
826	Tyr	O–P–O str		[17, 38]
789		C, T Backbone O–P–O sym		[17, 36, 40]
782		U, C, T Ring. Br		[17, 37]
753		T Ring. Br		[17, 36]
730	Ring. Br Try	A (C–C, ring mode)	C–N head Group	[17, 36, 37]
686		G (Ring. Br)		[17, 36]
668		T, G		[17, 36]
649	C–C twist Tyr			[36, 37]
622	C–C twist Phe			[36, 37]

approximately 1095 cm<sup>-1</sup> [8]. In addition to this the spectra for the nucleus (1020–1160 cm<sup>-1</sup> region) illustrated *n* in Fig. 4c shows an additional peak at 1055 cm<sup>-1</sup>, which can be attributed to a C–O stretching vibration from nucleotides, however, the possibility of a contribution from C–N stretch from Phenylalanine cannot be ruled out [27]. Based on the peak fitted data it has been possible to show significant differences between the Raman active bands in the cytoplasm and the nucleus. This highlights that the cytoplasm

consists of significantly more proteins and lipids than the nucleus, whereas the nucleus contains a greater contribution from DNA and RNA as expected [9, 13]. The results obtained here also correspond closely to those observed by Chan et al. [28]. It should also be noted that small variations were observed in the spectra collected from the nuclei within different cells. It has been observed by others that during differentiation the nucleus volume shrinks and there is a significant decrease in the RNA and DNA levels [19]. As

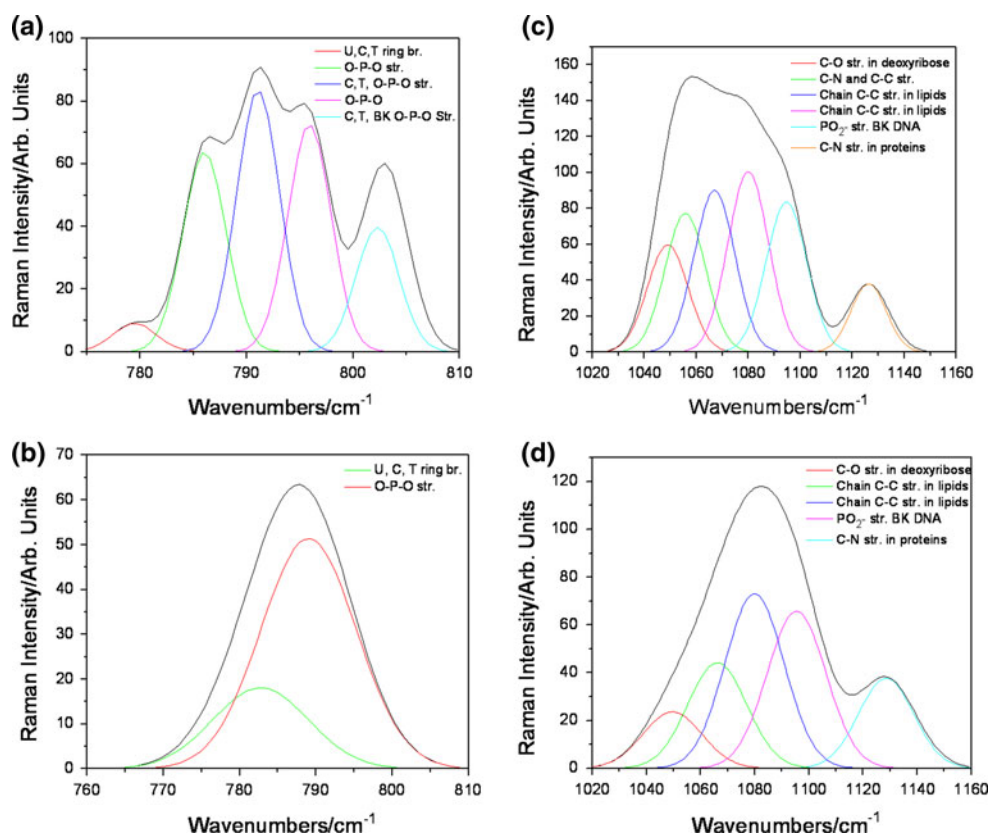


**Fig. 4** Peak fitting of the 770–810  $\text{cm}^{-1}$  region corresponding to the **a** nucleus, **b** cytoplasm and the 1020–1160  $\text{cm}^{-1}$  region corresponding to the **c** nucleus, **d** cytoplasm

such it would be expected that the Raman spectra obtained from the analysis of the nuclei from a population of differentiating cells may show some variation. Small differences were also observed between the spectra collected from the cytoplasm of different cells. This could have been attributed to differences to when the cells were analysed during their cell cycle, a non-homogeneous distribution of the various cellular components, problems relating to laser spot focus, or any combination of these.

### 3.2.2 Cell cluster analysis

A typical averaged Raman spectrum for a BAEC cluster on a fused silica substrate is presented in Fig. 5 ( $n = 3$ ). The averaged spectra shows contributions from the collective cellular components, i.e., proteins, lipids, nucleic acids, and carbohydrates, etc. and are comparable to those observed previously by others [7, 8, 13, 29]. These include commonly identified protein peaks, such as those observed at 1004  $\text{cm}^{-1}$  for phenylalanine. Other typical protein peaks are identified between 1128–1450 and 1600–1660  $\text{cm}^{-1}$  as expected [13, 17]. Some of the spectra contained peaks indicative of DNA and RNA were also identified at 782, 788, 1152, 1240–1345, and 1578  $\text{cm}^{-1}$ . Other vibrational bands

are identified between the 1190–1385  $\text{cm}^{-1}$  region, which are indicative of both nucleic acids and proteins present [26]. Peaks indicative of carbohydrates can also be seen around 1080–1095, 1420–1480, 1340  $\text{cm}^{-1}$  along with significant C–H stretching bands between 2800 and 3050  $\text{cm}^{-1}$  (not shown here). These bands are all typical of those observed previously in the single cell analyses [6, 30, 31].

The Raman spectra obtained from the cell clusters highlighted significant differences in some of the key peaks when compared to those obtained for the single cell analysis, specifically the 1095  $\text{cm}^{-1}$  peak associated with DNA phosphodiester bonds. The low intensity of the peak at 1095  $\text{cm}^{-1}$  could be as a result of numerous factors, including a lack of sensitivity given the optical platform employed for this part of the study, damage to the cells on the outer surface of the cluster due to handling, differences due to when the cells were analysed during their cell cycle, problems relating to laser spot focus on the cell cluster, or any combination of these. With specific reference to the issues relating to cell cycle, it would be preferable to ensure that the cells were at the same phase of the cell cycle [26]. However, in a real application area, such as the expansion of a cell population for use in a tissue engineered product, it is unlikely that all of the cells would be at the

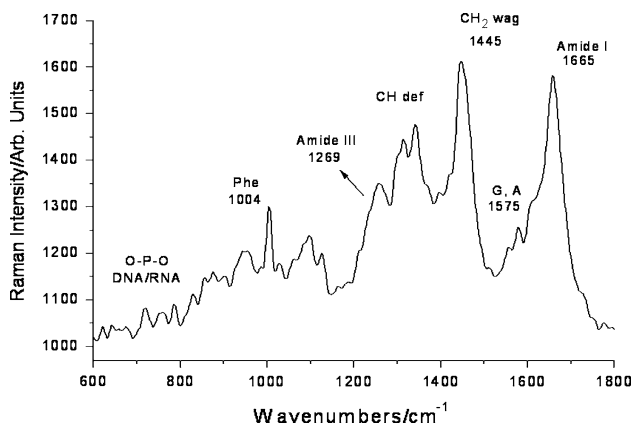


**Fig. 5** Raman spectrum of a bovine aortic endothelial cell cluster on a fused silica substrate with exposure time of 120 s

same phase of the cell cycle all of the time and as such, any method used to analyse the cells should be capable of coping with such situations. The results presented here clearly indicate that the Raman system employed here using a 100  $\mu\text{m}$  laser spot size at focus can be utilised to monitor cell behaviour in real-time and in a non-destructive and non-invasive manner. Certainly it is considered that the system incorporating the 100  $\mu\text{m}$  laser spot size is more appropriate for process monitoring in potential tissue engineering applications. This is due to the fact that the system takes an average spectrum from a large number of cells rather than analysing individual cells (or areas within individual cells). As such, the data obtained is more representative of the cell population as a whole. It also provides a technique to analyse a larger number of cells more rapidly than before, when compared to approaches using confocal or micro-Raman platforms. However, confocal or micro-Raman techniques would be a more appropriate optical platform to employ in the analysis of cell monolayers, whereas analysis using a 100  $\mu\text{m}$  laser spot size at focus (or larger) may be more appropriate in the analysis of cells growing in a 3D culture environment on a scaffold. This clearly shows that further work is required in order to understand the limitations of different optical platforms that may have utility in tissue engineering applications, particular those platforms that employ laser spot sizes greater than 100  $\mu\text{m}$ . To date, knowledge relating to such studies in the literature is limited.

#### 4 Conclusion

Selecting the ideal optical platform for the analysis of live cells is essential for obtaining both valid and reproducible results. This study clearly highlights the versatility of different Raman optical platforms to analyse populations of primary BAECs. It is evident from the work presented here

that this can be achieved using a Raman system that is not microscope based and is suited to high throughput screening of large populations of cells. As yet neither Raman platform employed has been optimised for use in a clinical or manufacturing environment for the expansion of healthy cell populations. In particular, issues relating to sensitivity and the capability to analyse samples in a non-destructive manner have not been fully addressed. However, the work undertaken here does show significant potential for the use of Raman spectroscopy in tissue engineering applications and will be the subject of further detailed investigations by the authors.

**Acknowledgments** The authors would like to express their gratitude to the EPSRC for funding this project (EP/C534247/1 (Remedi) Regenerative Medicine—A New Industry). The authors would also like to thank the Department of Education and Learning Northern Ireland (DEL NI) for additional funding for the project and Horiba Scientific for the use of the Confocal XploRa Raman Microscope.

#### References

- Langer R, Vacanti JP. Tissue engineering. *Science*. 1993;260(5110): 920–6.
- Ikada Y. Tissue engineering: fundamentals and applications. Amsterdam: Elsevier Science Ltd.; 2006.
- Polak JM, Bishop AE. Stem cells and tissue engineering: past, present, and future. In: *Annals of the New York Academy of Sciences, Skeletal Development and Remodeling in Health, Disease, and Aging*, vol. 1068; 2006. p. 352–66.
- Nottingham I, et al. In situ non-invasive spectral discrimination between bone cell phenotypes used in tissue engineering. *J Cell Biochem*. 2004;92(6):1180–92.
- Mather ML, Morgan SP, Crow J. Meeting the needs of monitoring in tissue engineering. *Regen Med*. 2007;2:145–60.
- Nottingham I. Raman spectroscopy cell-based biosensors. *Optic Biosen*. 2007;7(8):1343–58.
- Nottingham I, Hench LL. Raman microspectroscopy: a noninvasive tool for studies of individual living cells in vitro. *Expert Rev Med Devices*. 2006;3:215–34.
- Nottingham I, Verrier S, Haque S, Polak JM, Hench LL. Spectroscopic study of human lung epithelial cells (A549) in culture: living cells versus dead cells. *Biopolymers*. 2003;72(4):230–40.
- Swain RJ, Stevens MM. Raman microspectroscopy for non-invasive biochemical analysis of single cells. *Biochem Soc Trans*. 2007;035(3):544–9.
- Yang Y, Dubois A, Qin X, Li J, Haj A. Investigation of optical coherence tomography as an imaging modality in tissue engineering. *Phys, Med Bio*. 2006;51:1649–59.
- Kraft C. Bioanalytical applications of Raman spectroscopy. *Anal Bioanal Chem*. 2004;378(1):60–2.
- Puppels GJ, Garritsen HS, Segers-Nolten GM, de Mul FF, Greve J. Raman microspectroscopic approach to the study of human granulocytes. *Biophys J*. 1991;60(5):1046–56.
- Nottingham I, Hench LL. In situ characterisation of living cells by Raman spectroscopy. *Spectroscopy*. 2002;16(2):43–51.
- Short KW, Carpenter S, Freyer JP, Mourant JR. Raman spectroscopy detects biochemical changes due to proliferation in Mammalian Cell Cultures. *Biophys J*. 2005;88(6):4274–88.

15. Swain RJ, Jell G, Stevens MM. Non-invasive analysis of cell cycle dynamics in single living cells with Raman micro-spectroscopy. *J Cell Biochem*. 2008;104(4):1427–38.
16. Uzunbajakava N, Manen HWJV, Otto C. Raman microscopy on single cells: imaging of apoptosis and phagocytosis at high resolution. *GIT Lab J Eur*. 2004;8(3):22–5.
17. Verrier S, Notingher I, Polak JM, Hench LL. In situ monitoring of cell death using Raman microspectroscopy. *Biopolymers*. 2004;74(1–2):157–62.
18. Jell G, Notingher I, Tsigkou O, Notingher P, Polak JM, Hench LL, Stevens MM. Bioactive glass-induced osteoblast differentiation: a noninvasive spectroscopic study. *J Biomed Mater Res Part A*. 2008;86A(1):31–40.
19. Notingher I, Bisson I, Polak JM, Hench LL. In situ spectroscopic study of nucleic acids in differentiating embryonic stem cells. *Vib Spectrosc*. 2004;35(1–2):199–203.
20. Notingher I, Jell G, Notingher P, Bisson I, Tsigkou O, Polak JM, Stevens MM, Hench LL. Multivariate analysis of Raman spectra for in vitro non-invasive studies of living cells. *J Mol Struct*. 2005;744–747:179–85.
21. Gentleman E, Swain RJ, Evans ND, Boonrunsiman S, Jell G, Ball MD, Shean TAV, Oyen ML, Porter A, Stevens MM. Comparative materials differences revealed in engineered bone as a function of cell-specific differentiation. *Nat Mater*. 2009;8(9):763–70.
22. Huang M, Karashima T, Yamamoto K, Hamaguchi H. Molecular-level investigation of the structure, transformation, and bioactivity of single living fission yeast cells by time- and space-resolved Raman spectroscopy. *Biochemistry*. 2005;44(30):10009–19.
23. Huang Y-S, Karashima T, Yamamoto M, Hamaguchi H. Molecular-level pursuit of yeast mitosis by time- and space-resolved Raman spectroscopy. *J Raman Spectrosc*. 2003;34(1):1–3.
24. Booyse FM, Sedlak BJ, Rafelson ME. Culture of arterial endothelial cells: characterization and growth of bovine aortic cells. *Thromb Diath Haemorrh*. 1975;34(3):825–39.
25. Schwartz SM. Selection and characterization of bovine aortic endothelial cells. *In Vitro*. 1978;12(12):966–80.
26. Boyd AR, Burke GA, Meenan BJ. Monitoring cellular behaviour using Raman spectroscopy for tissue engineering and regenerative medicine applications. *J Mater Sci: Mater Med*. 2010;21(8):2317–24.
27. Uzunbajakava N, Lenferink ATM, Kraan YM, Willekens B, Vrensen GFJM, Greve J, Otto C. Nonresonant raman imaging of protein distribution in single human cells. *Biopolymers*. 2003;72(1):1–9.
28. Chan JW, Taylor DS, Thompson DL. The effect of cell fixation on the discrimination of normal and leukemia cells with laser tweezers Raman spectroscopy. *Biopolymers*. 2009;91(2):132–9.
29. Nohe A, Hassel S, Ehrlich M, Neubauer F, Sebald W, Henis YI, Knaus P. The mode of bone morphogenetic protein (BMP) receptor oligomerization determines different BMP-2 signaling pathways. *J Biol Chem*. 2002;277:5330–8.
30. Notingher I, Hench LL. A bio-photonics system for rapid in vitro testing of cells and ceramics. *Key Eng Mater*. 2005;284286:531–6.
31. Notingher I, Selvakumaran J, Hench LL. New detection system for toxic agents based on continuous spectroscopic monitoring of living cells. *Biosens Bioelectron*. 2004;20(4):780–9.
32. Lakshmi RJ, Kartha VB, Murali Krishna C, Solomon JG, Ullas G, Uma Devi P. Tissue Raman spectroscopy for the study of radiation damage: brain irradiation of mice. *Radiat Res*. 2009;157(2):175–82.
33. Naumann D. FT-infrared and FT-Raman spectroscopy in biomedical research. In: Gremlich HU, Yan B editors. *Infrared and Raman spectroscopy of biological materials*, New York: Marcel Dekker; 2001. p. 323–377.
34. Carter EA, Edwards HGM. Biological Applications of Raman spectroscopy. In: Gremlich HU, Yan B, editors. *Infrared and Raman Spectroscopy of Biological Materials*. New York: Marcel Dekker; 2001. p. 421–476.
35. Omberg KMO, Jill C, Zhang SL, Freyer JP, Mourant JR, Schoonover JR. Raman spectroscopy and factor analysis of tumorigenic and non-tumorigenic cells. *Appl Spectrosc*. 2002;56(7):813–9.
36. Overman SA, Aubrey KL, Reilly KE, Osman O, Hayes SJ, Serwer P, Thomas GJ Jr. Conformation and interactions of the packaged double-stranded DNA genome of bacteriophage T7. *Biospectroscopy*. 1998;4(S5):S47–56.
37. Kendall C, Stone N, Shepherd N, Geboes K, Warren B, Bennett R, Barr H. Raman spectroscopy, a potential tool for the objective identification and classification of neoplasia in Barrett's oesophagus. *J Pathol*. 2003;200(5):602–9.
38. Mahadevan-Jensen A, Richards-Kortum R. Raman spectroscopy for the detection of cancers and precancers. *J Biomed Opt*. 1996;1(1):31–70.
39. Borchman D, Tang D, Yappert MC. Lipid composition, membrane structure relationships in lens and muscle sarcoplasmic reticulum membranes. *Biospectroscopy*. 1999;5(3):151–67.
40. Rajani C, Kincaid JR, Petering DH. Raman spectroscopy of an O(2)-Co(II)bleomycin-calf thymus DNA adduct: alternate polymer conformations. *Biophys Chem*. 2001;94(3):219–36.